NAR Cancer, 2025, **7**, zcaf035
https://doi.org/10.1093/narcan/zcaf035
DNA Damage Sensing and Repair

Androgen receptor inhibition extends PARP inhibitor activity in prostate cancer models beyond BRCA mutations and defects in homologous recombination repair

Giuditta Illuzzi[1,†], Alessandro Galbiati[1,5,†], Anna D. Staniszewska[1], Robert Hanson[2,3], Chrysiis Michaloglou[1], Sophie L. Cooke[1], Karolina Uznańska[4], Maja Białecka[4], Kamil Solarczyk[4], Harveer S. Dev[3], Charlie E. Massie[3], Mark R. Albertella[1], Elisabetta Leo[1], Josep V. Forment[1,*], Mark J. O'Connor[1,*]

[1]Bioscience, Oncology R&D, AstraZeneca, 1 Francis Crick Avenue, Cambridge CB2 0AA, UK
[2]Translational Medicine, Oncology R&D, AstraZeneca, 1 Francis Crick Avenue, Cambridge CB2 0AA, Cambridge, UK
[3]Early Cancer Institute, Cancer Research UK Cambridge Centre; Department of Oncology, University of Cambridge Hutchison-MRC Research Centre, Adrian Way, Cambridge CB2 0AH, UK
[4]intoDNA S.A., Bobrzyńskiego 14, 30-348 Krakow, Poland
[5]Present address: Nerviano Medical Sciences, Viale Pasteur 10, Nerviano (MI), Italy

[*]To whom correspondence should be addressed. Email: josep.forment@astrazeneca.com
Correspondence may also be addressed to Mark J. O'Connor. Email: mark.j.oconnor@astrazeneca.com
[†]These authors contributed equally to this work.

Abstract

Clinical trials show benefit of the combination of poly(ADP-ribose) polymerase inhibitors (PARPi) with androgen receptor (AR) pathway inhibitors (ARPi) in metastatic, castration-resistant prostate cancer. While benefit was evident in patients with tumours harbouring mutations in homologous recombination repair (HRR) genes, improved outcomes were also observed in the absence of such alterations. Although there is literature linking AR with DNA repair, the basis of the interaction between the AR and PARP is unclear. We show that benefit of the combination of ARPi and PARPi in prostate cancer models with no HRR mutations requires ARPi-responsive cells and a PARPi with PARP1-trapping activity, and does not involve an effect of PARPi treatment in modulating AR transcription. Combination benefit is driven by an increase in DNA double-strand breaks and micronuclei formation, which is not due to a control of HRR gene transcription by the AR. Also, we uncover a novel role of PARP1 modulating AR recruitment to chromatin in the presence of DNA damage. These data shed light on the interplay between PARP1 and the AR in dealing with genotoxic insults and provide a mechanism-of-action consistent with the clinical benefit of the combination of PARPi and ARPi in patients with prostate cancer.

Graphical abstract

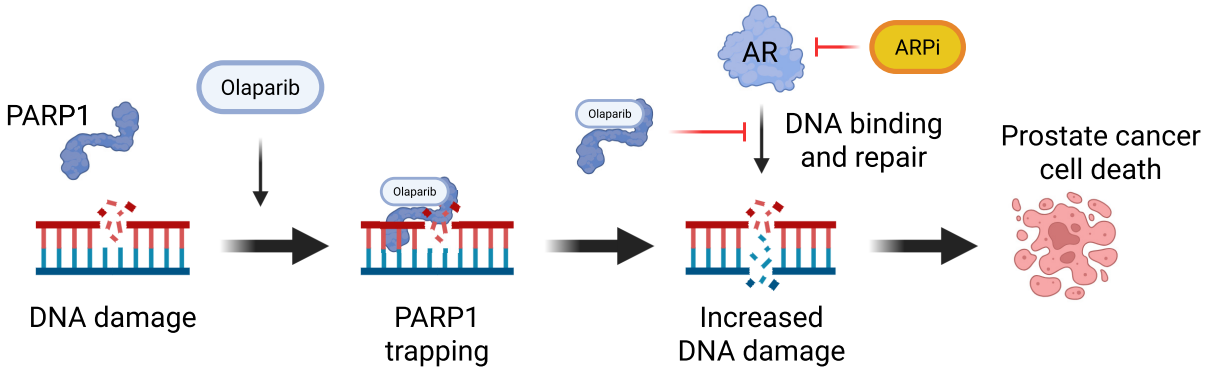

Created in BioRender. Forment, J. (2025) https://BioRender.com/uts17lt

Received: January 23, 2025. **Revised:** July 30, 2025. **Accepted:** August 20, 2025
© The Author(s) 2025. Published by Oxford University Press.
This is an Open Access article distributed under the terms of the Creative Commons Attribution-NonCommercial License (https://creativecommons.org/licenses/by-nc/4.0/), which permits non-commercial re-use, distribution, and reproduction in any medium, provided the original work is properly cited. For commercial re-use, please contact reprints@oup.com for reprints and translation rights for reprints. All other permissions can be obtained through our RightsLink service via the Permissions link on the article page on our site—for further information please contact journals.permissions@oup.com.

Introduction

The androgen receptor (AR) is the predominant driver of prostate cancer biogenesis and progression. In the metastatic or recurrent state, prostate cancer is normally treated with anti-hormonal therapy or androgen-deprivation therapy. These include first generation AR-pathway inhibitors (ARPi), such as bicalutamide or nilutamide that target AR translocation to the nucleus and prevent downstream signaling. Second-generation ARPi (also known as novel hormonal agents, or NHAs) such as enzalutamide, apalutamide or darolutamide, further improve upon this mechanism, while the ARPi/NHA abiraterone acetate prevents androgen biosynthesis [1].

Poly(ADP-ribose) polymerase (PARP) inhibitors (PARPi) are approved as monotherapy for patients with certain tumour types displaying defects in the DNA homologous recombination repair (HRR) pathway, exemplified by those harbouring mutations in the *BRCA1* or *BRCA2* genes [2]. PARPi approved for monotherapy use (olaparib, niraparib, rucaparib and talazoparib) both inhibit PARP enzyme activity and trap PARP proteins at DNA single-strand breaks leading to the accumulation of potentially cytotoxic DNA double-strand breaks (DSB) in HRR deficient backgrounds [3–5]. It has been shown that prostate tumours harbour defects in DNA repair genes, most commonly *BRCA2* and *ATM* [6]. As such, different clinical trials in metastatic, castration-resistant prostate cancer (mCRPC), have shown the benefit of PARPi monotherapy in patients that progressed on ARPi treatment and whose tumours harbour HRR mutations, leading to their approval in this setting [7, 8].

A phase 2 clinical trial investigated the efficacy of the PARPi olaparib in mCRPC in combination with the ARPi abiraterone, showing benefit in unselected mCRPC populations [9]. These observations have recently been confirmed in a phase 3 study of olaparib in combination with abiraterone (PROpel study; NCT03732820), and this PARPi-ARPi combination is also supported by trials testing talazoparib in combination with enzalutamide (TALAPRO-2 study, NCT03395197). As perhaps expected, patients with tumours harbouring mutations in *BRCA1*, *BRCA2* or other HRR genes, benefitted most from the PARPi plus ARPi combination, but a benefit in patients harbouring tumours with no such mutations was also reported [10, 11]. Links between AR activity and the DNA repair machinery have been previously identified [12–16] and are believed to contribute to the observed clinical benefit of combining androgen deprivation therapy with radiation treatment [17]. However, the molecular mechanisms behind this interplay are still unclear, particularly in the case of PARPi combinations [18]. Here, we sought to gain additional insights by assessing the combination of ARPi plus PARPi in preclinical *in vitro* and *in vivo* prostate cancer models and better understand the key determinants of combination activity.

Materials and methods

Cell lines and compounds

The following cell lines were originally obtained from ATCC: LNCAP, C4-2, DU145, 22rv1, VCAP. The isogenic cell lines CWR22Pc-R1-AD1 and CWR22Pc-R1-D567, were obtained by Dr. Scott Dehm from University of Minnesota (USA). The castrate resistant LNCAP95 (also indicated as LNCAP CR) was obtained by Dr Meeker from John Hopkins University (USA). LNCAP ATM KO clones were as previously described [19]. Cell line identification was validated using the CellCheck assay (IDEXX Bioanalytics, Westbrook, ME, USA). All cell lines were validated free of virus and mycoplasma contamination using the MycoSEQ assay (Thermo Fisher Scientific, Waltham, MA, USA) or STAT-Myco assay (IDEXX Bioanalytics). All cell lines were grown in RPMI-1640 growth media (Corning 17–105-CV) supplemented with 10% fetal bovine serum (FBS) or, when indicated, 10% charcoal stripped FBS (ThermoFisher Scientific, 12 676 029) and 2 mM glutamine. Olaparib, enzalutamide, veliparib, talazoparib, ATM inhibitor (AZD1390) were made by AstraZeneca (Cambridge, UK). Hydrogen peroxide solution was bought by Sigma (cat. No. H1009), methyl methane sulfonate was bought by Sigma (cat. No. 129 925). 5-alpha-dihydrotestosterone was bought by Sigma (cat. No. NMID680) and solubilized in ethanol.

Cell proliferation assay and combination benefit calculation

Cells in 384-well or 96-well plates were dosed using an Echo 555 (LabCyte, San Jose, CA, USA) or using the HP D300e Digital Dispenser (HP Life Science Dispensing), respectively. Cell viability pre- and post-treatment (6–8 days after treatment) was determined using CellTiter-Glo as per manufacturer's instructions (Promega, Madison, WI, USA; G7570). For the combination experiments data were converted to 0–200% growth inhibition in Genedata Screener as previously described [20] and synergy scores were calculated by comparison to the Loewe model of additivity [21]. For three biological repeats, synergy scores and IC50 values were calculated from growth curves averaged from two technical replicates. In the represented plots error bars are mean ± S.E.M for three biological replicates.

Colony formation assay

Cells were seeded in 24-well plates (1 500 cells/well) and incubated overnight. Drugs were dispensed by an automated digital D300 HP dispenser (Tecan) in titration dilutions, covering 0.1 nM – 10 μM range; each concentration was tested in triplicate and DMSO was used as untreated control. Plates were incubated at 37 °C, 5% CO_2 for 14 days, to allow colony formation. Cells were then fixed and stained with Blue-G-250 brilliant blue (#B8522-1EA, Sigma, reconstituted in 25% (v/v) methanol and 5% (v/v) acetic acid) for 15min then thoroughly washed with dH_2O. Plates were scanned with GelCount™ (Oxford OPTRONIX). Colonies were analyzed by total optical density measured with ImageJ software, using a 24-well plate ROI mask. Data analysis was performed by normalization on the vehicle treated of the respective plate set as 1. Data were plotted and IC50s were calculated with GraphPad Prism software.

RNA-seq

LNCAP cells (5 × 10e5) were seeded in 10 cm dishes and cultured for 3 days before treatment with compounds. Cell lysates were harvested following 8 h, 24 h and 72 h incubation with test compounds, via scraping cells into lysis buffer whilst on ice. RNA was extracted using Qiagen All-Prep kit following manufacturer's instructions (Qiagen, 2005) and quantified using Qubit RNA BR assay (Life technologies, 2012). 1 μg total RNA from each treatment condition was used as input for mRNA library preparation using the TruSeq RNA Li-

brary Prep Kit, following the manufacturer's protocol (Illumina). The final 36 sample libraries were pooled in groups of 12, forming three equimolar pools each at 10 nM concentration. Sample pools were submitted for paired-end sequencing (2 × 150bp) on 3 lanes of a HiSeq-4000. Pre-processing of raw read data, alignment and transcript counting was performed using STAR [22] and featureCounts tools [23]. Differential expression analysis was performed using the DESeq2 package in R [24]. Gene set enrichment analyses (GSEA) were performed on gene lists, ranked by log fold change with respect to DMSO controls, using fgsea package in R [25]. Significantly enriched biological pathways were identified through comparison against the Hallmark pathway signatures, from the MSigDB database [26].

RNA isolation and gene expression analysis by Fluidigm

Cells cultured in 96-well plates were dosed using the HP D300e Digital Dispenser (HP Life Science Dispensing) as indicated. Total RNA was isolated from cells in 96-well plates using the Qiagen FastLane Cell Probe Kit (QIAGEN, 216 413), according to the manufacturer's instructions to a final volume of 40 μL per well, at the indicated time point after treatment.

For Fluidigm analysis cells were snap frozen in RLT buffer and then processed as described in [27]. RNA extraction was performed using the RNeasy Plus Mini Kit and RNase-free DNase Kit (Qiagen) on the Qiacube HT instrument (Qiagen) according to manufacturer's instructions. RNA concentration was measured using the NanoDrop ND8000 (NanoDrop). 50 ng of RNA was used to perform reverse transcription with a Reverse Transcription Master Mix (Fluidigm), and cDNA was then pre-amplified (14 cycles) using a pool of TaqMan primers (Life Technologies) and Preamp Master Mix (Fluidigm). Gene expression analysis was then performed using the 96.96 Fluidigm Dynamic arrays according to the manufacturer's instructions. Data were collected and analyzed using Fluidigm Real-Time PCR Analysis software. dCt was calculated by subtacting Average Ct of housekeeping genes from each Ct. An average dCt for the control group was calculated and subtracted from dCt to calculate negative ddCt (NegddCt). 2^negative ddCt was used to calculate Fold Change. P values were calculated by performing a student's t-test on the negative ddCt values. Data were plotted using Spotfire software. Taqman probes used for the Fluidigm analysis are available as on Table 1.

DNA damage and cell cycle analysis by immunofluorescence

Cells were seeded in imaging-quality 96-well plates (Phenoplates, PerkinElmer #6 055 300). Compounds were added using a D300 HP dispenser (Tecan) from compound stocks dissolved in DMSO, in duplicate for each condition. Plates were incubated for the specified time. During the last 30 min of incubation, EdU was added to cells at a final concentration of 10 μM, and then processed for immunofluorescence. For immunofluorescence analysis, cells were washed and fixed in 4% paraformaldehyde (PFA) for 15 min at RT and then permeabilized in PBS + 0.2% Triton X-100 for 10 min at RT. Blocking was performed using PBG: 0.5% BSA + 0.2% gelatin from cold water fish skin (Sigma, cat no. G7765) in PBS for 1 h at RT. EdU Click-IT reaction was performed following the manufacturer's instructions (Thermofisher). Cells were then washed 3 times with PBG; primary antibodies were incubated overnight at 4°C (γH2AX, Merck Millipore, 05–636, diluted 1:5 000. RAD51 antibody, Bioacademia 70–002, rabbit, diluted 1:7 000), followed by secondary antibody (anti-mouse, Alexa Fluor 594 (Thermo, A21099, 1:2 000) and DAPI (ThermoFisher, D1306, diluted 1 μg/ml) for 30 min at RT. Image acquisition and analysis was done with the scanR high content screening platform (Olympus, Evident). 40x objectives were used for image acquisition; 25–36 fields were acquired. For foci analysis "spots detector module" was used. For cell cycle analysis DAPI and EdU signals were used to gate for G1, S, G2 cell cycle phases. For micronuclei analysis an image analysis protocol generated with cellSens(Evident) was used.

STRIDE assay for detection of DSBs (dSTRIDE)

Direct detection of DSBs was performed at the intoDNA laboratory using the dSTRIDE procedure, as previously described [28]. In brief, after overnight fixation of cells in ethanol at -20C, modified nucleotide analogues (BrdU) were incorporated at the sites of DSBs and then detected using appropriate primary antibodies. Next, secondary antibodies with conjugated oligonucleotides and connector oligonucleotides were used and ligated to form a circular DNA template. Finally, rolling circle reaction occurred followed by hybridization of short fluorescently labelled oligonucleotides to the amplicon. STRIDE procedure was followed by DAPI nucleus counterstaining (Thermo Scientific 62 248), PCNA IF staining (anti-PCNA antibody Abcam ab29) and CellMask Deep Red cytoplasmic membrane staining (Invitrogen C10046). Fields of view (FOVs) for imaging were chosen randomly over the surface of the sample. The images were then acquired as 3D confocal stacks using Cell Discoverer 7 LSM 900 microscope, Zeiss. Nuclei were recognized based on DAPI staining. 3D masks were created for each recognized nucleus and its projection. Identification of STRIDE foci was based on 3D local maxima of fluorescence inside the nucleus masks. Only the foci localized inside the 3D masks were included in further data analysis.

Immunoblotting

Cells were lysed in RIPA buffer (Pierce Thermo) supplemented with protease inhibitors (Roche), phosphatase inhibitors (Sigma-Aldrich) and benzonase (Merck, #103 773). After 30 min of incubation in ice the lysates were centrifuged at + 4°C for 15 min and supernatant were kept for sample loading. NuPAGE™ LDS Sample Buffer (ThermoFisher Scientific, NP0008) and NuPAGE™ Sample Reducing Agent (ThermoFisher Scientific, NP0004) were added to the samples. Equal amounts of whole cell lysates were separated on 4–12% Bis-Tris NuPAGE gels and analysed by standard immunoblotting. All immunoblots are representative of experiments that were performed at least twice independently. All antibodies used are described in Table 2.

Subcellular fractionation

Cells were plated in 10 cm dishes and treated as indicated. Plates were washed once with PBS and cells were scraped in 1 mL PBS 1x. 20% of the cell suspension was centrifuged and resuspended in RIPA buffer (Pierce Thermo) as described above to obtain the total cell lysate, while the remaining part of the sample was submitted to cellular fractionation using the Subcellular Protein Fractionation Kit for Cultured Cells

Table 1. List of Taqman probes used for the Fluidigm studies

Gene name	Description	Gene ID	Category	Probe number
ABCC4	ATP-binding cassette, sub-family C (CFTR/MRP), member 4	10 257	AR	Hs00988717_m1
AR	androgen receptor	367	AR	Hs00171172_m1
CAMKK2	calcium/calmodulin-dependent protein kinase kinase 2, beta	10 645	AR	Hs00198032_m1
EAF2	ELL associated factor 2	55 840	AR	Hs00218407_m1
FKBP5	FK506 binding protein 5	2289	AR	Hs01561006_m1
FOXA1	forkhead box A1	3169	AR	Hs04187555_m1
GNMT	glycine N-methyltransferase	27 232	AR	Hs00219089_m1
KLK3	kallikrein-related peptidase 3	354	AR	Hs02576345_m1
NKX3.1	NK3 homeobox 1	4824	AR	Hs00171834_m1
NNMT	nicotinamide N-methyltransferase	4837	AR	Hs00196287_m1
SGK1	serum/glucocorticoid regulated kinase 1	6446	AR	Hs00178612_m1
STK39	serine threonine kinase 39	27 347	AR	Hs00202989_m1
TMPRSS2	transmembrane protease, serine 2	7113	AR	Hs01120965_m1
AKT1	v-akt murine thymoma viral oncogene homolog 1	207	CELL CYCLE/PROLIFERATION	Hs00178289_m1
BAX	BCL2-associated X protein	581	CELL CYCLE/PROLIFERATION	Hs00180269_m1
CCNA2	cyclin A2	890	CELL CYCLE/PROLIFERATION	Hs00996788_m1
CCNB1	cyclin B1	891	CELL CYCLE/PROLIFERATION	Hs99999188_m1
CCND1	cyclin D1	595	CELL CYCLE/PROLIFERATION	Hs00765553_m1
CCNE2	cyclin E2	9134	CELL CYCLE/PROLIFERATION	Hs00372959_m1
CDKN1A	cyclin-dependent kinase inhibitor 1A (p21, Cip1)	1026	CELL CYCLE/PROLIFERATION	Hs00355782_m1
MTOR	mechanistic target of rapamycin (serine/threonine kinase)	2475	CELL CYCLE/PROLIFERATION	Hs00234508_m1
PCNA	proliferating cell nuclear antigen	25 737	CELL CYCLE/PROLIFERATION	Hs00427214_g1
PTEN	phosphatase and tensin homolog	5728	CELL CYCLE/PROLIFERATION	Hs01920652_s1
TP53	tumour protein p53	7157	CELL CYCLE/PROLIFERATION	Hs01034253_m1
ATM	ataxia telangiectasia mutated	472	DDR	Hs01112355_g1
ATR	ataxia telangiectasia and Rad3 related	545	DDR	Hs00992123_m1
BRCA1	breast cancer 1, early onset	672	DDR	Hs01556193_m1
BRCA2	breast cancer 2, early onset	675	DDR	Hs01037421_m1
CHEK1	checkpoint kinase 1	1111	DDR	Hs00967506_m1
CHEK2	checkpoint kinase 2	11 200	DDR	Hs00200485_m1
FANCA	Fanconi anemia, complementation group A	2175	DDR	Hs01116668_m1
FANCD2	Fanconi anemia, complementation group D2	2177	DDR	Hs00276992_m1
FEN1	flap structure-specific endonuclease 1	2237	DDR	Hs00748727_s1
MRE11A	MRE11 meiotic recombination 11 homolog A (S. cerevisiae)	4361	DDR	Hs00967443_m1
PARP1	poly (ADP-ribose) polymerase 1	142	DDR	Hs00242302_m1
PPARG	peroxisome proliferator-activated receptor gamma	5468	DDR	Hs01115511_m1
PRKDC	protein kinase, DNA-activated, catalytic polypeptide	5591	DDR	Hs00179161_m1
RAD21	RAD21 homolog (S. pombe)	5885	DDR	Hs00366721_mH
RAD50	RAD50 homolog (S. cerevisiae)	10 111	DDR	Hs00990023_m1
RAD51C	RAD51 paralog C	5889	DDR	Hs00427442_m1
RNASEH2A	ribonuclease H2, subunit A	10 535	DDR	Hs00197370_m1
XRCC4	X-ray repair complementing defective repair in Chinese hamster cells 4 (double-strand-break rejoining)	7518	DDR	Hs00243327_m1
XRCC6	X-ray repair complementing defective repair in Chinese hamster cells 6	2547	DDR	Hs01922655_g1
ACTB	actin beta	60	Housekeeping	Hs01060665_g1
GAPDH	glyceraldehyde-3-phosphate dehydrogenase	2597	Housekeeping	Hs02758991_g1
IPO8	importin 8	10 526	Housekeeping	Hs00183533_m1
POLR2A	RNA polymerase II subunit A	5430	Housekeeping	Hs01108271_g1
YWHAZ	tyrosine 3-monooxygenase/tryptophan 5-monooxygenase activation protein zeta	7534	Housekeeping	Hs00237047_m1

Table 2. Antibodies for immunoblotting

Target	Host species	Cat. Number.	Provider	Working dilution
γH2AX	Mouse	05–636	Merck Millipore	1:2000
Vinculin	Mouse	V9131	Sigma	1:2000
Histone H3	Mouse	3638	Cell Signalling	1:2000
CyclinA2	Mouse	ab38	Abcam	1:500
RAD51	Rabbit	70–001	BioAcademia	1:7000
AR	Rabbit	5153	Cell Signalling	1:1000
AR	Mouse	MA5-13 426	ThermoFisher	1:500
PARP1	Rabbit	9532	Cell Signalling	1:1000
GAPDH	Rabbit	2118	Cell Signalling	1:1000
RAD51	Rabbit	ABE257	Merck Millipore	1:500
Lamin A/C	Rabbit	2032	Cell Signalling	1:1000
pRAD50 (p-S635)	Rabbit	14 223	Cell Signalling	1:1000
PAR	Rabbit	83 732	Cell Signalling	1:1000
PARP2	Rabbit	39 743	Active Motif	1:1000
pKAP1 (p-S824)	Rabbit	A300-867A	Bethyl Laboratories	1:1000
ATM	Rabbit	Ab32420	Abcam	1:1000
pATM (p-S1981)	Rabbt	Ab81292	Abcam	1:1000

(ThermoFisher Scientific, 78 840) and processed according to manufacturer's instructions. Equal volumes of each fraction were loaded on SDS gels and processed for immunoblotting as described above. Quantifications were performed with ImageJ image analysis software. For each subcellular fraction AR protein signals were normalized on loading controls (H3 or LaminA/C) and calculated as ratio to DMSO.

Statistical analysis

Results are shown as mean ± standard error of the mean (s.e.m) or standard deviation (SD) as indicated. P-value was calculated by Student's two-tailed t-test or with the indicated statistical test, using Graphpad Prism software v8.3.1. Statistical significance is indicated as follows: * $p \leq 0.05$, ** $p \leq 0.01$, *** $p \leq 0.001$, **** $p \leq 0.0001$.

Gene silencing with siRNA transfection

Cells were seeded in 10 cm plates and transfected with siPARP1 (Horizon Discovery Ltd, Cambridge, UK L-006656–03–0005), siPARP2 (Horizon Discovery Ltd, Cambridge, UK L-010127–02–0005) or non-targeting siCTRL (Horizon Discovery Ltd, Cambridge, UK, D-001810–0X), using the RNAiMax transfection reagents (ThermoFisher Scientific, 13 778 075), following manufacturer instructions, at a final concentration of 10 nM. Cells were incubated with the siRNA, RNAiMAX, OPTIMEM (ThermoFisher Scientific, 31 985 070) and the appropriate cell culture medium for 48 h before processing for protein levels and cellular subcellular fractionation assays.

Immunoprecipitation

The chromatin fraction (50 μL) obtained following the cellular fractionation method described above was diluted in the 500 μL of the IP buffer (20 mM Tris-HCl pH 7.5, 150 mM NaCl, 2 mM MgCl2, 0.5% Triton X-100, 10% glycerol, cOmplete™ Protease Inhibitor Cocktail (Roche). 1:10 of the sample was kept aside as input, while the rest of the sample was incubated over-night at 4°C, on a rotating wheel, with 2.5 μg of anti-IgG antibody (ThermoFisher Scientific, 31 235) or 2.5 μg of anti-AR antibody (CST, 5153). The following day 50 μL per sample of Protein A Dynabeads (10002D) were blocked with PBS + BSA 5mg/mL for 30 min and then washed 3x in the IP buffer. Then, 50 μL of beads were added to each sample and incubated for 3 h at 4°C, on a rotating wheel. Then, beads were washed 3x in the IP buffer. Finally, the samples were eluted in 50 μL 2x NuPAGE™ LDS Sample Buffer (ThermoFisher Scientific, cat. No. NP0008) + NuPAGE™ Sample Reducing Agent (ThermoFisher Scientific, cat. No. NP0004). Sample Inputs and IP were immunoblotted as described above.

In-vitro PARylation assay and PAR-binding assay with purified proteins

Purified recombinant PARP1 (6His 6Lys TEV PARP1 1–1014 (Hp155), produced in SF21 insect cell baculovirus vector) and recombinant AR N-terminal (N-His6-TEV-hARV (G142-G627), produced in SF21 insect cell baculovirus vector) were produced by AstraZeneca. AR C-terminal fragment (650–920) was bought from Abcam (ab82124), BSA was used as control (Sigma). For the in-vitro PARP1-dependent PARylation assay, 2.5 μg BSA, 2.5 μg AR N-term or 2.5 μg AR C-term were incubated with the following reaction mix for 30 min at RT: PARP1 (800 ng), dsDNA oligo (5 μg, previously annealed, M3 5′ACTTGATTAGTTACGTAACGTTATGATTGA3′, M4 5′TCAATCATAACGTTACGTAACTAATCAAGT3′;), NAD + 1mM, Tris HCl pH 7.5 50 mM and water to a total volume of 50 μL per reaction. The reaction was then loaded on a gel and immunoblotted with the primary antibody anti-PAR diluted 1:1000 (CST #83 732), as described above. For the PAR binding assay, 2.5 μg of BSA, AR N-terminal and AR C-terminal were mixed with NuPAGE™ LDS Sample Buffer (ThermoFisher Scientific, cat. No. NP0008) + NuPAGE™ Sample Reducing Agent (ThermoFisher Scientific, cat. No. NP0004) and loaded on a on 4–12% Bis-Tris NuPAGE gels. Following gel running and transfer, the membrane was incubated with 100 nM purified PAR polymer (Trevigen, 4336–100–01) for 1 h at RT. Following extensive washing with PBS, the membrane was then processed as a regular western blot and incubated with anti-PAR antibody diluted 1:1000 (CST #83 732)

Xenograft studies

Xenograft studies were performed at Axis Bioservices (Coleraine, UK) in accordance with UK Home Office legislation,

the Animal Scientific Procedures Act 1986, Axis Bioservices Animal Welfare and Ethical Review Committee, and the AstraZeneca Global Bioethics policy. Animals were housed in IVC cages (up to 5 per cage) with individual mice identified by tail mark. All animals were allowed free access to a standard certified commercial diet and sanitized water during the study. The holding room was maintained under standard conditions: room temperature at 20–24°C, humidity at 30–70% and a 12h light/dark cycle used. LNCAP or C4-2 cells (10 million with 50% Matrigel) were implanted subcutaneously into the dorsal flank of male non-obese diabetic (NOD) severe combined immunodeficiency (SCID) mice (aged 5–8 weeks, weighing approximately 25–30g) (Axis Bioservices). Tumours were measured (length x width) three times weekly by bilateral Vernier caliper measurements and tumour volume was calculated using the elliptical formula (width × width × length)/2. Animal bodyweight and tumour condition were monitored throughout the study. Mice were randomized into treatment groups when mean tumour volume reached approximately 0.15 cm3. Animals were treated from the day after the randomization. Olaparib (AZD2281, AstraZeneca), and enzalutamide (ChemShuttle) were administered by oral gavage (PO) at 10 mL/kg final dose volume. Olaparib was formulated in 10% DMSO, 30% HB-β-CD. Enzalutamide was formulated in 5% DMSO: 95% Methylcellulose (0.5% w/v) with 0.1% Tween-80. Tumour growth inhibition from start of treatment was assessed by comparison of the mean change in tumour volume of the control and treated groups and represented as percent tumour growth inhibition (TGI, when TV ≥ starting TV). Statistical significance was evaluated using a one-tailed t test. Statistical significance is indicated as follows: * $p \leq 0.05$, ** $p \leq 0.01$, *** $p \leq 0.001$.

VCAP ATM KO cell line generation

Lentiviral production and transduction was performed in HEK293T cells as described in [19]. To establish the VCAP stably Cas9 expressing cell line, VCAP cells were transduced with lentivirus expressing the pKLV2-EF1a-BsdCas9-W (Addgene #67 978) vector. The cell pools were then selected with Blasticidine for 3 passages and Cas9 expression was confirmed by western blot. To establish VCAP ATM KO cells, 0.3 × 106 VCAP Cas9 cells were seeded in 6-well plates, and cells were transduced with the lentivirus containing the sgRNA targeting ATM as described in [19]. ATM knockout cell pools were analysed by immunoblot and TIDE sequencing to assess the KO efficiency.

Results

Combination activity between PARPi and ARPi is more pronounced in ARPi-responsive cell lines treated with a PARPi that has effective PARP1-trapping ability

To better understand combination activity between ARPi and PARPi, we performed *in vitro* efficacy studies in a panel of prostate cancer cell lines. We selected cell lines highly sensitive to ARPi treatment (LNCAP, VCAP), others with an intermediate phenotype (C4-2, R1-AD1) and some completely unresponsive to ARPi challenge (R1-D567, LNCAP 95, DU145) (Supplementary Fig. S1A). As expected, given the lack of biallelic, pathological mutations in *BRCA1*, *BRCA2*, *ATM* or other HRR genes, none of the cell lines tested displayed high levels of single agent PARPi sensitivity as observed in HRR mutated backgrounds. Specifically, all half maximal inhibitory concentrations (IC_{50}) for olaparib in the panel were in the μM range (Supplementary Fig. S1A), compared to the low nM IC_{50} values reported for HRR deficient cell lines [19, 29].

Combinations were assessed between olaparib and enzalutamide, and synergy scores [21] were derived. Interestingly, scores suggestive of additive combination benefit (synergy score between 0–5) tended to be higher in ARPi-responding cell lines (Fig. 1A; Supplementary Fig. S1B-C). To determine whether this increased combination benefit would also track with PARPi activity, we assessed synergy scores in two of the ARPi-responsive cell lines (LNCAP and VCAP) where we inactivated the *ATM* gene through CRISPR-Cas9 gene editing (Supplementary Fig. S1D), as loss of ATM activity has been shown to increase PARPi sensitivity *in vitro* [19, 30]. As shown in Figs 1B-C, combination activity was increased in the *ATM* KO backgrounds, compared to their *ATM* WT counterparts (Supplementary Fig. S1E-F). Importantly, this increased combination benefit required a PARPi with good PARP-trapping ability (olaparib), as it could not be reproduced by using the weak PARP trapper, veliparib (Fig. 1D) [29]. To determine combination benefit in a different way, we assessed the effect of adding a fixed dose of enzalutamide (response curve is provided in Supplementary Fig. S1G), to a dose-response colony-forming assay experiment with three different PARPi in the C4-2 cell line. In line with our combination matrices data, we observed a decrease of the IC_{50} values of the PARP trappers, olaparib and talazoparib when combined with enzalutamide, while no significant change was observed with the weaker PARP trapper, veliparib (Fig. 1E). Interestingly, the greatest fold change in IC_{50} of the PARPi used when combined with enzalutamide was with olaparib (Fig. 1F).

Previous studies have reported that PARPi could synergize with androgen-deprivation therapies by inhibiting a positive transcriptional activation role of PARP1 on the AR pathway [13]. For this reason, we were surprised by the lack of combination activity between enzalutamide and veliparib, since this is a potent inhibitor of PARP enzyme activity, in spite of it having weak PARP-trapping ability. Since the reported mechanism of action for the AR-cofactor role of PARP1 does not require PARP1 trapping [13], we decided to explore this previously proposed mechanism further. We assessed the effect of olaparib on the transcriptional profile of LNCAP cells in the presence or absence of ARPi challenge. While enzalutamide treatment had a strong effect at downregulating the expression of AR signature genes, olaparib treatment did not show any modulation of this signature and did not further increase the inhibitory effect of enzalutamide on the expression of this gene set (Fig. 1G).

Taken together, these results show that combination of PARPi and ARPi *in vitro* is more pronounced in ARPi-responsive cell lines and requires PARPi with PARP1-trapping ability. In addition, combination benefit is higher in genetic backgrounds with increased sensitivity to PARPi, exemplified here by prostate cancer cell lines defective in the *ATM* gene. In addition, our data in Fig. 1E–G also indicate that PARPi ARPi combination efficacy does not involve any effect of PARPi on AR transcriptional signaling as previously proposed.

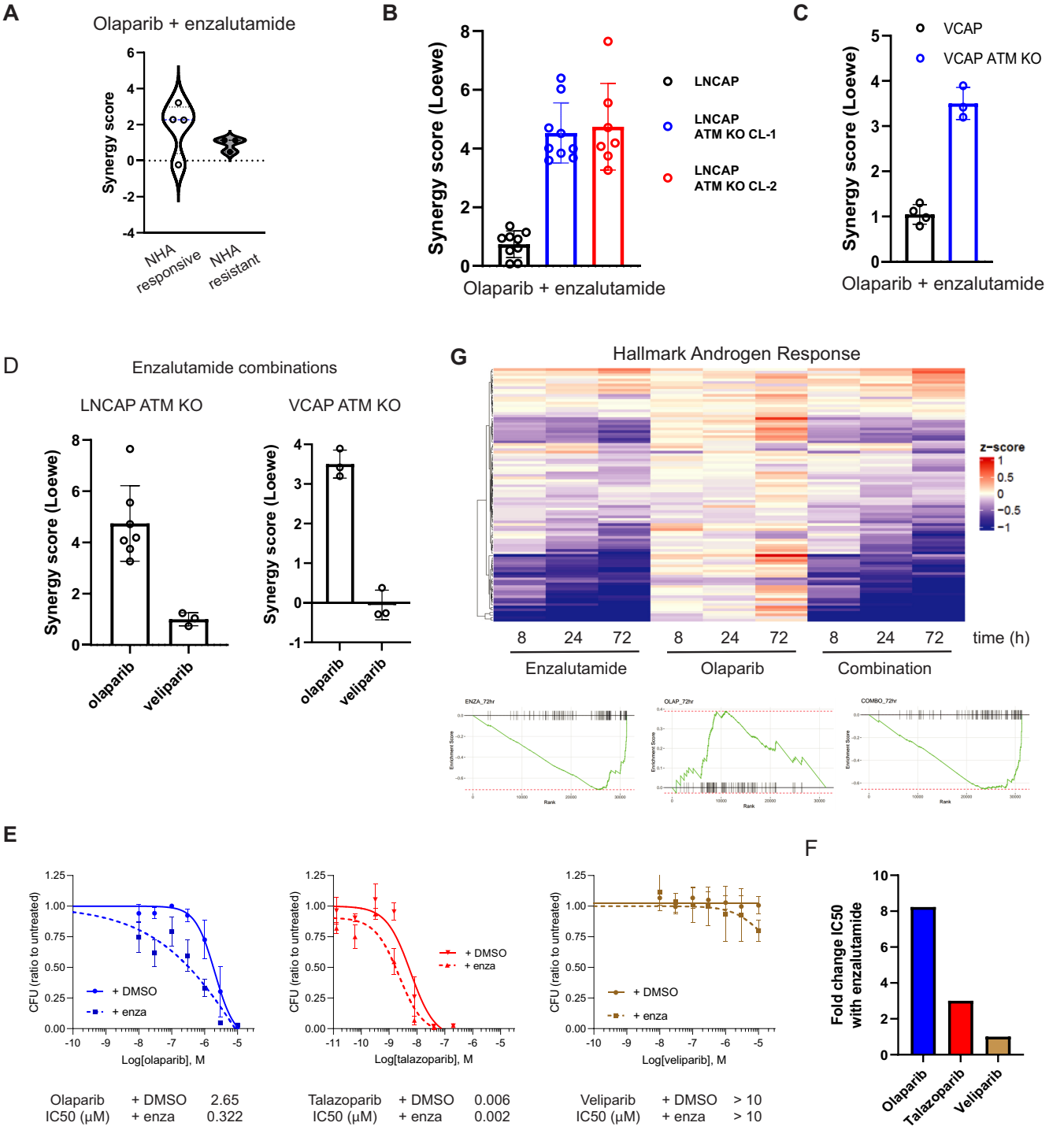

Figure 1. (**A**) Combination activity between olaparib and enzalutamide in a panel of prostate cancer cell lines. Each dot represents a cell line (see Supplementary Fig. S1B). (**B**) Combination activity between olaparib and enzalutamide in LNCAP and two different isogenic LNCAP *ATM* KO clones. (**C**) Combination activity between olaparib and enzalutamide in VCAP and a VCAP *ATM* KO pool. (**D**) Combination activity between the PARPi, olaparib or veliparib, and enzalutamide in LNCAP *ATM* KO (left panel) and VCAP *ATM* KO (right panel) backgrounds. (**E**) Clonogenic survival assay of C4-2 cells treated with a dose range of different PARPi – olaparib (left panel), talazoparib (middle panel), and veliparib (right panel) – combined with DMSO or a fixed dose of enzalutamide (0.3 μM). IC50 values for the combinations are provided at the bottom of each graph. (**F**) IC50 fold change for the PARPi used in panel (E) between DMSO and enzalutamide combinations. (**G**) RNA-seq differential expression levels in the AR hallmark gene signature in LNCAP treated with enzalutamide, olaparib, or their combination (top panel) and leading-edge analysis (bottom panels). In all panels, a minimum of two biological replicates for each condition are presented.

Combination of PARPi with ARPi generates more DNA damage than either single agent

The increased benefit of the combination of PARPi with ARPi was particularly evident when using PARPi with PARP1-trapping activity, pointing towards a DNA damage component driving the combination effect. For this reason, we decided to measure DNA damage by quantifying the accumulation of micronuclei in C4-2 cells treated with enzalutamide, olaparib or their combination. Micronuclei formation is a key measurement of genomic instability and a possible consequence of DNA damage [31]. Importantly, combination of enzalutamide with olaparib increased the presence of micronuclei-positive cells compared to either single agent (Fig. 2A). To confirm that the accumulation of micronuclei could be a consequence of DNA damage, we measured DNA DSB formation in C4-2 cells treated with enzalutamide, PARPi or their combination using dSTRIDE [28]. While enzalutamide treatment did not significantly increase DSB formation, the PARP-trapping PARPi olaparib did, with no significant effect observed with the weaker PARP trapper, veliparib. Strikingly, combination of enzalutamide with olaparib further increased DSB accumulation, an effect that was not recapitulated by the veliparib combination (Fig. 2B; Supplementary Fig. S2). These data correlate with the effect of these combinations in C4-2 cell survival, where enzalutamide increased the efficacy of olaparib but not of veliparib (Fig. 1E).

Literature reports have suggested that use of ARPi in prostate cancer cell lines could generate a HRR deficient environment, which could explain the ARPi PARPi combination benefit and persistent DNA damage [15, 16]. To assess this, we measured nuclear focal accumulation of the key HRR recombinase RAD51 [32], as defects in RAD51 foci formation are a *bona fide* readout of HRR defects [19]. Olaparib treatment increased RAD51 foci formation in C4-2 cells (Fig. 2C), as expected in a cell line carrying no defined mutations in HRR genes. Surprisingly, combined treatment of olaparib with enzalutamide did not alter the ability of C4-2 cells to form RAD51 foci, suggesting that no functional defect in HRR was induced by ARPi treatment (Fig. 2C).

To better understand the discrepancy between our data and previously published observations, we evaluated RAD51 protein expression in VCAP and LNCAP cells, which are very sensitive to enzalutamide treatment, and in R1-AD1 and C4-2 cells, which show a more resistant phenotype (Supplementary Fig. S1A). Interestingly, RAD51 protein expression upon enzalutamide challenge was reduced in VCAP and LNCAP cells, while no effect was observed in R1-AD1 and C4-2 cells, despite enzalutamide treatment effectively downregulating protein expression of the AR target gene, *FKBP5*, in all cell lines (Fig. 2D). We confirmed these observations at the transcriptional level, as enzalutamide treatment caused significant downregulation of the expression of a set of AR-target genes in both LNCAP and R1-AD1 cells (Supplementary Fig. S3A), while it only consistently reduced expression of a set of genes involved in the DNA damage response (DDR) in the more sensitive LNCAP cell line (Supplementary Fig. S3B).

As expression of a number of DNA repair proteins is downregulated in the G1 phase of the cell cycle, and upregulated during the proliferation phases (S/G2) [33], we investigated the effect of enzalutamide treatment on the cell cycle distribution of these prostate cancer cell lines. Importantly, enzalutamide exposure for 48 h resulted in very low levels of actively replicating cells in VCAP and LNCAP cells, while much more modest reductions were observed in R1-AD1 and C4-2 cells (Supplementary Fig. S3C). This reduced proliferation index was also detected through reduced protein expression of the key S/G2 Cyclin A2 protein exclusively in VCAP and LNCAP cells (Fig. 2D). Further confirming these observations, enzalutamide treatment significantly reduced expression levels of genes involved in cell cycle regulation only in LNCAP cells (Supplementary Fig. S3B). To better understand the impact of cell cycle re-distribution over prolonged enzalutamide exposure, we performed a time course of RAD51 foci formation in the C4-2 cell line, as the strong cell cycle arrest observed in LNCAP and VCAP prevented further analyses beyond the 48 h time frame in these cell lines (Supplementary Fig. S3C). Such analyses showed that enzalutamide treatment did not prevent RAD51 foci formation in cells in S or G2 phases even after 7 days of enzalutamide exposure (Supplementary Fig. S3D), despite an effective reduction on proliferating cells (Supplementary Fig. S3E). This is important, as DNA damage accumulation in olaparib-treated cells was mainly restricted to cells in S/G2 (Supplementary Fig. S3F).

Collectively, these data suggest that rather than direct modulation of HRR genes by ARPi treatment, reduced expression of these genes is an indirect effect of enzalutamide challenge in ARPi-responsive cell lines due to changes in the proliferation status of the cells. This indirect effect of enzalutamide treatment on DDR and cell cycle gene expression, however, did not result in HRR deficiency, as highlighted by the ability of enzalutamide-treated cells to accumulate RAD51 protein at DNA damage sites over a prolonged time frame (Fig. 2C and Supplementary Fig. S3D).

Taken together, these results suggest that the increased efficacy of the ARPi PARPi combination in ARPi-responding cell lines is due to increased DNA damage accumulation in the form of DSBs, driven by the PARP-trapping activity of PARPi.

The AR is recruited to chromatin in the presence of DNA damage in a PARP1-dependent manner

A direct protein–protein interaction between PARP1 and the AR has been reported [34], so we decided to explore whether such interaction could be modulated in the presence of DNA damage. For that purpose, we performed protein immunoprecipitations of the AR bound to chromatin from C4-2 cells in the presence or absence of olaparib and / or methylmethane sulphonate (MMS), a DNA alkylating agent that causes DNA damage and strongly induces PARP1 activity. Interestingly, we could observe an interaction between PARP1 and the AR in the chromatin fraction of C4-2 cells, even in unchallenged conditions (Fig. 3A, lane 2), and this was increased when cells were treated with MMS (Fig. 3A, compare lanes 2 and 4) but weakened by the combination with olaparib (Fig. 3A, compare lanes 4 and 5). Somewhat surprisingly, the increased interaction between PARP1 and the AR upon MMS treatment was clearly driven by an increase of both PARP1 and the AR in the chromatin-bound fraction (see inputs on lanes 4 and 5 compared to lanes 2 and 3 on Fig. 3A). This is expected for PARP1, as MMS-induced DNA damage will increase PARP1 trapping on chromatin [29] (note that the reduction on PARP1 levels on Fig. 3A, lane 5 is driven by the fact that this is a co-immunoprecipitation where the bait is the AR; MMS treatment did induce effective PARP1 trapping, as

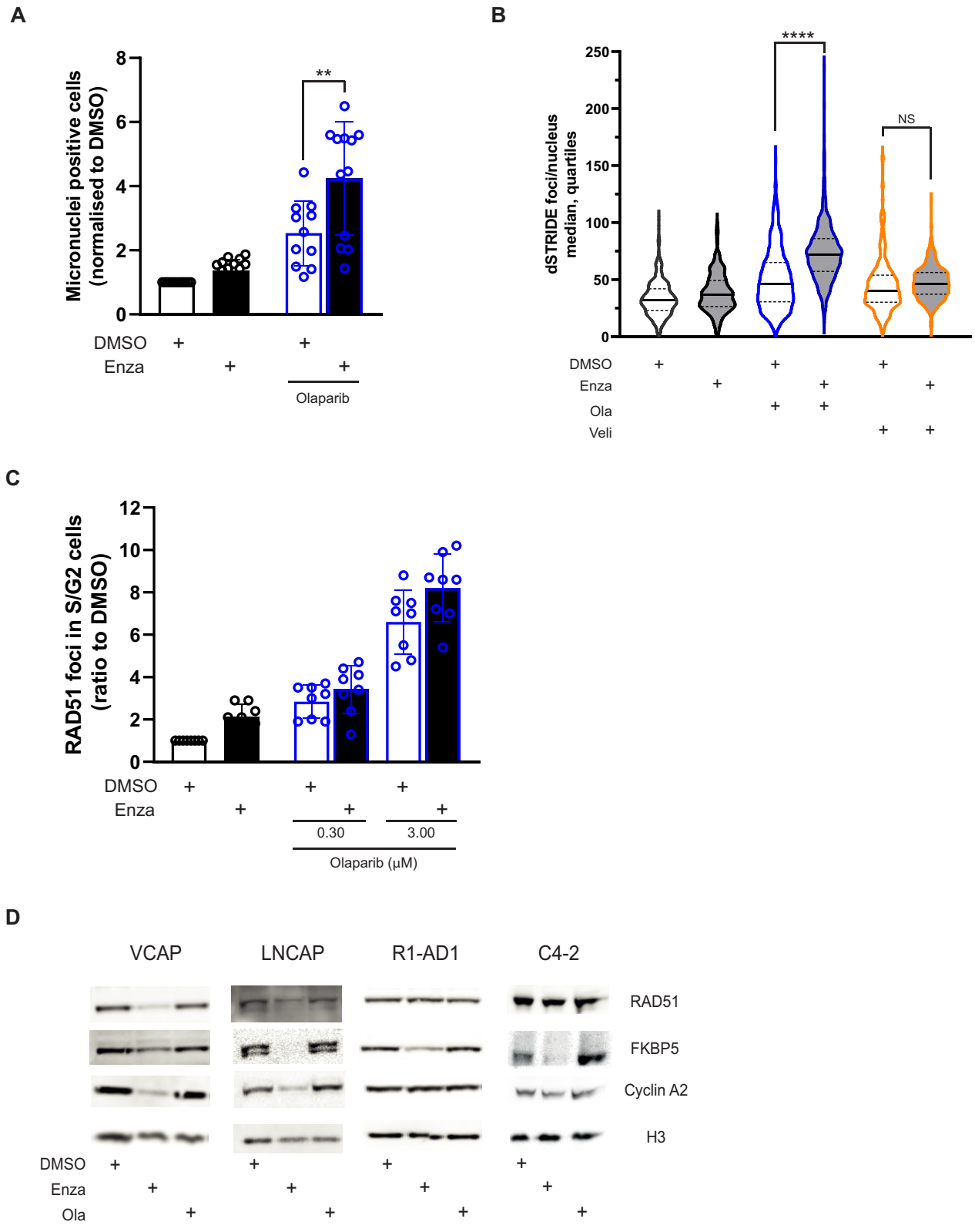

Figure 2. (**A**) Quantification of micronuclei in C4-2 cells treated with enzalutamide, olaparib, or their combination. Values are represented as ratios compared to DMSO-treated samples. (**B**) Quantification of dSTRIDE foci per nucleus in C4-2 cells treated for 72 h with 3 μM enzalutamide, PARPi (olaparib or veliparib, 1.8 μM), or their combination. (**C**) Quantification of RAD51 foci in C4-2 cells in S/G2 phase of the cell cycle treated for 48 h with enzalutamide (3 μM), olaparib or their combination. Values are represented as ratios compared to DMSO-treated samples. (**D**) FKBP5, Cyclin A2 and RAD51 protein levels in total cell lysates from VCAP, LNCAP, R1-AD1, or C4-2 cells treated with enzalutamide (3 μM), olaparib (3 μM), their combination or DMSO for 48 h. Histone H3 was used as loading control. In panels A–C, at least $n = 3$ independent biological replicates for each condition are presented.

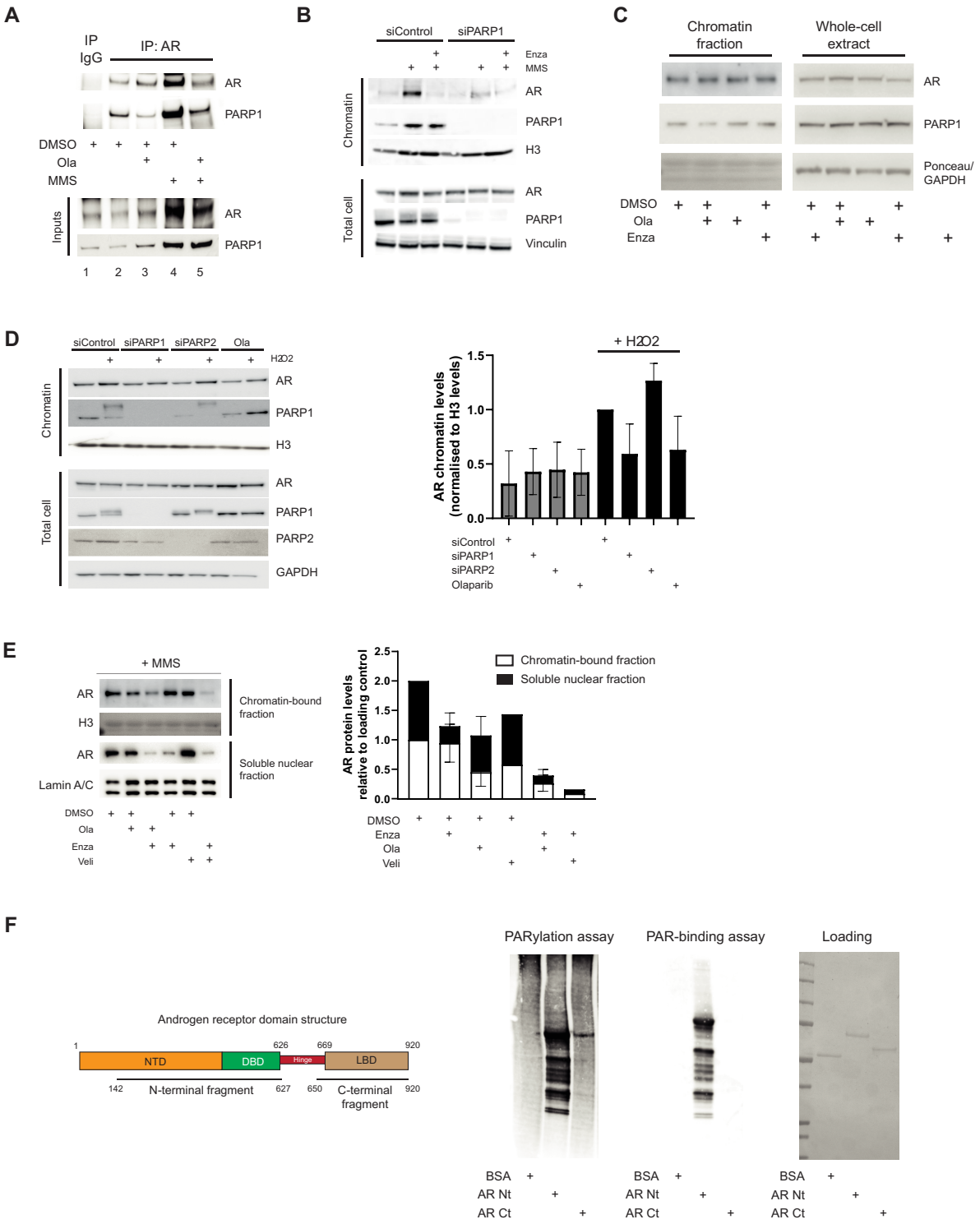

Figure 3. (**A**) AR and PARP1 levels in inputs (bottom panels) and AR immune-precipitation (IP) from the chromatin fraction of C4-2 cells treated with MMS (0.01%) for 3 h and pre-treated or not with olaparib 3 μM for 2 h before MMS treatment. (**B**) AR and PARP1 enrichment in the chromatin fraction in LNCAP cells treated with MMS (0.01%) for 3 h and pre-treated with enzalutamide (3 μM) or vehicle control for 16 h. Treatments were added after 48 h incubation with siRNA against PARP1 or a control sequence. (**C**) AR and PARP1 enrichment in the chromatin fraction in LNCAP cells pre-treated with olaparib (3 μM), enzalutamide (3 μM), their combination or vehicle control for 48 h. (**D**) AR and PARP1 enrichment in the chromatin fraction in C4-2 cells pre-treated with olaparib (3 μM) or vehicle control for 2 h before H_2O_2 treatment (1 mM) for 30 min. Treatments were added after 72 h of incubation with siRNA against PARP1, PARP2 or a control sequence. Left panel: representative western blot images. Right panel: quantification of three independent biological replicates. (**E**) AR nuclear distribution in chromatin-bound or soluble nuclear fractions of LNCAP cells treated with MMS 0.01% for the last 4 h after pre-treatment with enzalutamide, olaparib, or veliparib (all at 3 μM) as indicated. Left panel: representative western blot images. Right panel: quantification of three independent biological replicates for olaparib and one for veliparib. (**F**) PARylation assays with AR *N*-term or *C*-term fragments (encompassing domains highlighted on the left figure). Equal amounts of BSA or AR fragments (right panel) were used for a biochemical PARP1-dependent PARylation assay (left panel) or PAR-binding assay (middle panel). NTD = *N*-terminal domain; DBD = DNA-binding domain; LBD = ligand-binding domain.

observed in the input) but it is an unexpected result for the AR. We performed a chromatin-fractionation experiment in LNCAP cells treated or not with MMS in the presence or absence of enzalutamide and observed increased AR recruitment to chromatin after MMS treatment that was reduced by enzalutamide (Fig. 3B, lanes 1–3). Importantly, this MMS-induced AR recruitment to chromatin was also affected by PARP1 downregulation using small-interference RNA (siRNA) (Fig. 3B, compare lanes 2 and 5). Olaparib exposure did not affect AR chromatin recruitment in the absence of MMS treatment (Fig. 3B, compare lanes 1 and 4; Fig. 3C), in agreement with the observed lack of effect of PARPi on AR-dependent transcription in the absence of exogenous DNA damage (Fig. 1G).

These results were confirmed in a chromatin fractionation experiment in C4-2 cells treated with hydrogen peroxide (H_2O_2), another potent inducer of PARP1 activity [29]. Here, downregulation of PARP1, and not of PARP2, diminished H_2O_2-induced AR recruitment to chromatin, which was recapitulated by olaparib treatment (Fig. 3D). In line with the results using siRNA to inactivate PARP1, PARPi treatment reduced the amount of chromatin-bound AR after MMS treatment regardless of the PARP1-trapping ability of the PARPi used (Fig. 3E).

Given the physical interaction between PARP1 and the AR, we explored whether the AR could be a direct substrate of PARP1. For that purpose, we purified two different fragments of the AR protein, covering most of the amino acid sequence, and incubated them in the presence of purified PARP1, double-stranded DNA and NAD+, the necessary PARylation cofactor. As shown in Fig. 3F, PARP1 was able to PARylate the N-terminal fragment of the AR. In addition, we could also observe that the same N-terminal fragment of the AR has the ability to bind PAR chains (Fig. 3F).

Collectively, these data show that PARP1 and the AR directly interact, and that PARP1 can PARylate the N-terminal fragment of the AR, which can also bind PAR chains. In addition, the AR is recruited to chromatin in the presence of DNA damage in a PARP1-dependent manner.

Combination activity of PARPi and NHAs in prostate cancer xenograft models

Given the *in vitro* efficacy and DNA damage data generated in ARPi-responsive cell lines, we explored *in vivo* responses to the combination of olaparib with enzalutamide. In LNCAP xenografts, while enzalutamide or olaparib monotherapies had no significant anti-tumour effect, combination therapy resulted in significant tumour growth inhibition (TGI; Fig. 4A). In C4-2 xenografts, enzalutamide treatment had no significant anti-tumour effect, while olaparib monotherapy resulted in modest TGI. Importantly, combination of enzalutamide with olaparib showed a trend towards enhanced TGI (Fig. 4B). These *in vivo* experiments highlight that, in these particular xenograft models where enzalutamide monotherapy was not effective at the doses used, combination benefit may be mostly driven by DNA damage induction and impaired AR chromatin recruitment caused by olaparib treatment, further enhanced by the addition of enzalutamide. Taken together, these results show that combination of ARPi with PARPi can result in improved efficacy over monotherapies in prostate cancer xenograft models with no HRR defects.

Discussion

PARP inhibitors have demonstrated a clear benefit in HRR-deficient cancers, whether in defined BRCA mutated ovarian, breast, pancreatic or prostate cancers, or in broader HRR gene mutated (HRRm) or HRR-deficient (HRD) cancers defined by genomic scarring criteria. There are still valid questions about the activity of PARPi beyond HRD, particularly as monotherapy. However, the combination of PARPi with ARPi in prostate cancers has been demonstrated in both preclinical non-HRD models, as well as in the clinic in non-BRCA, non-HRR deficient (i.e. HRR proficient) tumours. The mechanism of action of the PARPi ARPi combination behind this activity has been less clear.

In this study, we have shown that the combination of PARPi and ARPi in prostate cancer cell models requires some level of response to ARPi and is further enhanced in the presence of mutations that lead to greater levels of PARPi efficacy. Importantly, we also show that this combination benefit relies on the ability of the PARPi to trap PARP on damaged DNA, and it is not linked to an effect of PARPi treatment on the expression of AR-driven genes. Accordingly, the combination benefit can be explained by an increase in the accumulation of DNA damage in the form of DNA DSBs when PARPi are combined with ARPi. Of note, we report here that this is not due to ARPi treatment generating an HRR deficient environment, and this is in agreement with a recent publication [35]. Moreover, we unveil a second component to this combination mechanism of action in the form of the requirement of PARP1 enzymatic activity for the recruitment of the AR to chromatin in the presence of DNA damage.

All these results can therefore be summarized as follows. In untreated conditions (Fig. 5A), the presence of endogenous DNA damage in prostate cancer cells leads to PARP1 recruitment to chromatin. PARP1 then PARylates itself, the surrounding chromatin and nuclear AR (in abundance in the nucleus in the presence of hormonal signals) to help AR recruitment to chromatin, which in turn will be important to facilitate DNA repair and cell survival. In the presence of ARPi treatment and a PARP-trapping PARPi (Fig. 5B), PARP1 gets trapped on DNA, increasing DNA damage during replication, and at the same time diminishes AR chromatin binding by inhibiting AR PARylation. ARPi treatment further impairs AR chromatin binding by reducing the total amount of AR in the nucleus. The combination of PARPi and ARPi thus results in an increased amount of DNA damage and leads to enhanced prostate cancer cell death, even in HRR-proficient prostate cancer cells. Importantly, the intrinsic sensitivity of the cancer cells to the PARPi or ARPi single agent effects will determine which of the different mechanisms of action (AR signaling blockade; PARPi-induced DNA damage; AR-dependent, PARPi-induced DNA damage repair) will be primarily driving the efficacy of the combination.

This model can help explain the clinical data generated so far with combinations of PARPi and ARPi in prostate cancer and given the importance of the PARP trapping and DNA damage accumulation mechanism for the efficacy of the combination, it explains the lack of benefit of the addition of the weak PARP trapper, veliparib, to the abiraterone regime [36]. This mechanism is also the basis of the improved benefit of the combination in HRR mutated backgrounds, including those with mutations in BRCA genes, where PARPi-induced DNA damage will be higher [10, 11, 37]. In non-HRR mutated tu-

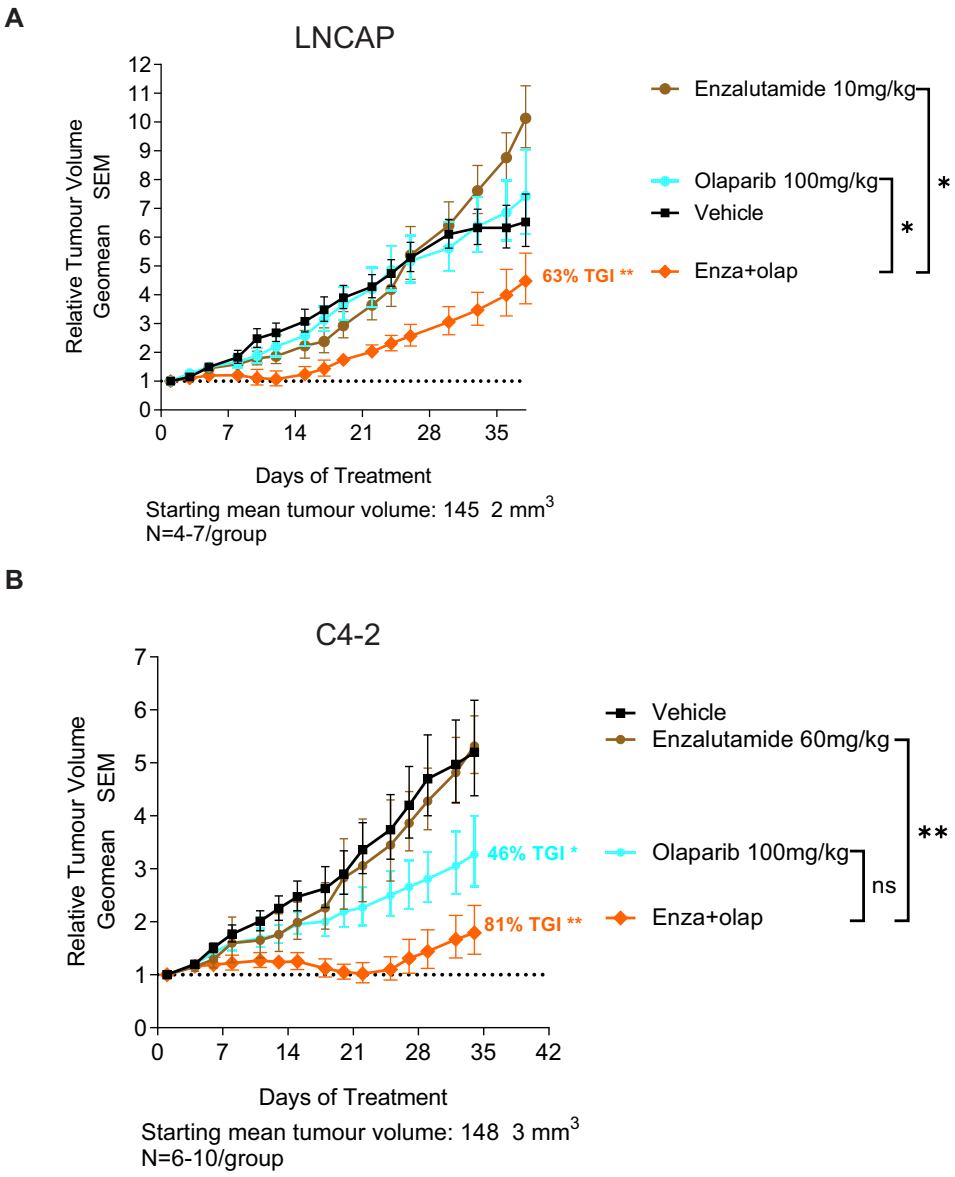

Figure 4. (**A**) Anti-tumour efficacy *in vivo* in LNCAP xenograft tumour model treated orally with olaparib (100 mg/kg BID) or enzalutamide (10 mg/kg QD) as monotherapies or in combination. (**B**) Anti-tumour efficacy *in vivo* in C4-2 xenograft tumour model treated orally with olaparib (100 mg/kg BID) or enzalutamide (60 mg/kg QD) as monotherapies or in combination. Graphs depict geomean tumour volume ± SEM and percent tumour growth inhibition (TGI). Statistical significance was evaluated compared with the vehicle or combination group using a one-tailed t test (*, $P \leq 0.05$; **, $P \leq 0.01$; ***, $P \leq 0.001$).

mours, this model predicts that being able to maintain effective PARP trapping over the course of the treatment will be needed to generate sufficient DNA damage accumulation to derive benefit in the presence of ARPi therapy. Importantly, dose reductions or dose interruptions of PARPi treatment are reported to result in reduced efficacy and progression on therapy [29]. In the PROpel clinical trial, olaparib was maintained at the full monotherapy dose of 300 mg twice a day in most patients (79.9%) and demonstrated benefit in patients with non-HRR mutated tumours when combined with abiraterone [10]. In contrast, the niraparib dose when combined with abiraterone in the MAGNITUDE clinical trial, required a dose-reduction of niraparib from its monotherapy dose (from 300 mg once daily to 200 mg once daily), and only demonstrated benefit in patients with HRR mutated tumours [38].

There are limitations to our work that warrant further investigation. For example, we still do not understand the details of how AR recruitment to chromatin in the presence of DNA damage leads to repair, particularly as we did not observe changes in the expression of DNA repair genes by ARPi treatment that cannot be explained by a short-term effect on cell cycle modulation. It is also unclear where the AR binds in response to DNA damage, and whether those chromatin regions are the ones containing DNA break sites. In addition, the mechanism proposed in Fig. 5 does not seem to be applicable to all preclinical prostate cancer models tested, as in some cases we did not detect combination benefit even in ARPi-responsive cell lines. In spite of this, the mechanism for the combination benefit observed between PARPi and ARPi based on increased DNA damage and inhibition

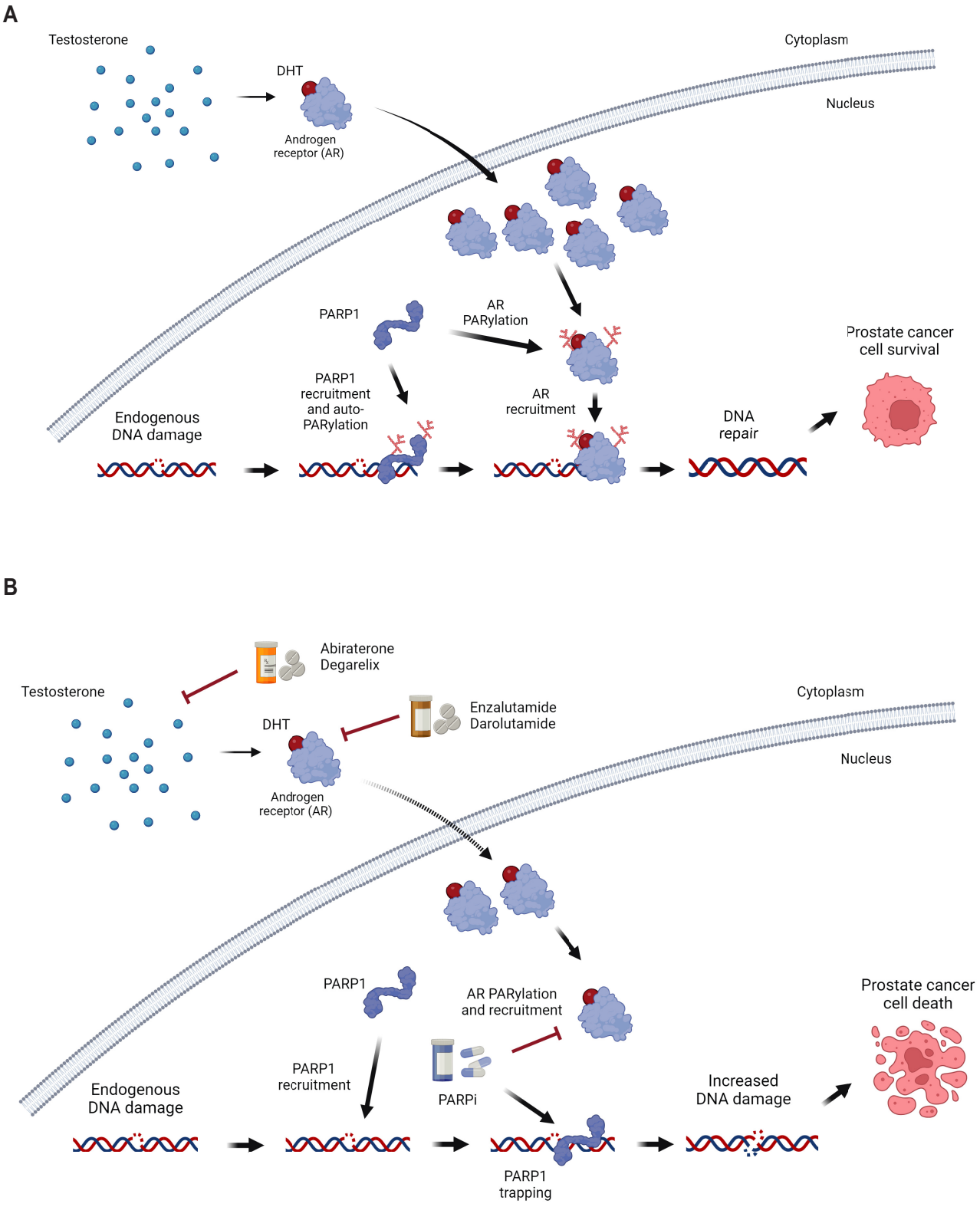

Figure 5. (**A**) Model to explain the combined action of PARP1 and the AR in facilitating DNA repair in prostate cancer cells. (**B**) Model to explain combination efficacy between PARPi and ARPi in prostate cancer treatment. DHT: dihydrotestosterone. Created in BioRender. Forment, J. (2024) https://BioRender.com/e98m788

of AR-dependent DNA damage repair does draw parallels with the reported clinical benefit of the combination of radiation therapy and androgen deprivation treatment [17]. In both cases, the key component is the increased persistence of DNA damage induced by either PARPi or ionizing radiation when the AR function is compromised [12, 14]. Unfortunately, there are very few prostate cancer preclinical models, in particular those representing relatively common clinical HRR genotypes, and this limits the ability to interrogate these mechanistic interactions in more depth. In order to attempt to overcome these preclinical limitations, a clinical study ASCERTAIN (NCT05938270) has been initiated, where the focus is on collection of pre- and post- treatment biopsies from monotherapy and combinations of the PARP1-selective PARPi, saruparib (AZD5305), and the ARPi darolutamide, with the aim of increasing further understanding of mechanisms of action between PARPi and ARPi. Results of the EvoPAR-Prostate-01 phase 3 clinical trial (NCT06120491), where the combination of saruparib with ARPi is being compared to ARPi monotherapy in metastatic, castration-sensitive prostate cancer patients, will shed further light into the interplay between PARPi and ARPi in both HRR mutated and not mutated settings.

Acknowledgements

The authors would like to thank Henson Lee Yu for his support uploading the RNAseq data on the GEO repository. The graphical abstract for this manuscript was created in BioRender. Forment, J. (2025) https://BioRender.com/uts17lt. Charlie E. Massie passed away before the paper was submitted and therefore was not able to approve the final accepted version and cannot be held accountable for the work post-publication.

Author contributions: G.I. and A.G. designed, performed and analysed *in vitro* experiments and contributed to manuscript writing; A.D.S. designed, performed, and analysed *in vivo* studies, and contributed to manuscript writing; R.H. designed, performed and analysed RNAseq experiments; C.M. performed and analysed Fluidigm expression experiments; S.C. assisted with chromatin fractionation experiments; K.U., M.B. and K.S. designed, performed and analysed STRIDE experiments; H.S.D. and C.E.M. designed, supervised and analysed RNAseq experiments; M.R.A. and E.L. supervised and contributed to the experimental plan and provided insights; M.O.C. supervised and contributed to the experimental plan, and contributed to manuscript writing; J.V.F. supervised and contributed to the design of the experimental plan, and wrote the manuscript. All authors contributed and approved the final version of the manuscript.

Supplementary data

Supplementary data is available at NAR Cancer online.

Conflict of interest

G.I., A.G., A.D.S., R.H., C.M., S.C., E.L., M.A., J.V.F., and M.J.O.C. are or were employees of AstraZeneca at the time of conducting these studies. Several authors hold stock or shares in AstraZeneca.

Funding

John Black Charitable Foundation, AstraZeneca UK, Cancer Research UK Cambridge Centre, and Prostate Cancer Foundation.

Data availability

The data underlying this article are available in the article and in its online supplementary material. RNA expression data can be accessed through the GEO accession number GSE303975.

References

1. Rice MA, Malhotra SV, Stoyanova T. Second-generation antiandrogens: from discovery to standard of care in castration resistant prostate cancer. *Front Oncol* 2019;**9**:801. https://doi.org/10.3389/fonc.2019.00801
2. Stewart MD, Merino Vega D, Arend RC *et al.* Homologous recombination deficiency: concepts, definitions, and assays. *Oncologist* 2022;**27**:167–74. https://doi.org/10.1093/oncolo/oyab053
3. Ray Chaudhuri A, Nussenzweig A. The multifaceted roles of PARP1 in DNA repair and chromatin remodelling. *Nat Rev Mol Cell Biol* 2017;**18**:610–21. https://doi.org/10.1038/nrm.2017.53
4. Lord CJ, Ashworth A. PARP inhibitors: synthetic lethality in the clinic. *Science* 2017;**355**:1152–8. https://doi.org/10.1126/science.aam7344
5. Pommier Y, O'Connor MJ, de Bono J. Laying a trap to kill cancer cells: PARP inhibitors and their mechanisms of action. *Sci Transl Med* 2016;**8**:362ps317. https://doi.org/10.1126/scitranslmed.aaf9246
6. Robinson D, Van Allen EM, Wu Y-M *et al.* Integrative clinical genomics of advanced prostate cancer. *Cell* 2015;**161**:1215–28. https://doi.org/10.1016/j.cell.2015.05.001
7. de Bono J, Mateo J, Fizazi K *et al.* Olaparib for metastatic castration-resistant prostate cancer. *N Engl J Med* 2020;**382**:2091–102. https://doi.org/10.1056/NEJMoa1911440
8. Fizazi K, Piulats JM, Reaume MN *et al.* Rucaparib or physician's choice in metastatic prostate cancer. *N Engl J Med* 2023;**388**:719–32. https://doi.org/10.1056/NEJMoa2214676
9. Clarke N, Wiechno P, Alekseev B *et al.* Olaparib combined with abiraterone in patients with metastatic castration-resistant prostate cancer: a randomised, double-blind, placebo-controlled, phase 2 trial. *Lancet Oncol* 2018;**19**:975–86. https://doi.org/10.1016/S1470-2045(18)30365-6
10. Clarke NW, Armstrong AJ, Thiery-Vuillemin A *et al.* Abiraterone and Olaparib for metastatic castration-resistant prostate cancer. *NEJM Evid* 2022;**0**:EVIDoa2200043.
11. Agarwal N, Azad AA, Carles J *et al.* Talazoparib plus enzalutamide in men with first-line metastatic castration-resistant prostate cancer (TALAPRO-2): a randomised, placebo-controlled, phase 3 trial. *The Lancet* 2023;**402**:291–303. https://doi.org/10.1016/S0140-6736(23)01055-3
12. Goodwin JF, Schiewer MJ, Dean JL *et al.* A hormone–DNA repair circuit governs the response to genotoxic insult. *Cancer Discov* 2013;**3**:1254–71. https://doi.org/10.1158/2159-8290.CD-13-0108
13. Schiewer MJ, Goodwin JF, Han S *et al.* Dual roles of PARP-1 promote cancer growth and progression. *Cancer Discov* 2012;**2**:1134–49. https://doi.org/10.1158/2159-8290.CD-12-0120
14. Polkinghorn WR, Parker JS, Lee MX *et al.* Androgen receptor signaling regulates DNA repair in prostate cancers. *Cancer Discov* 2013;**3**:1245–53. https://doi.org/10.1158/2159-8290.CD-13-0172
15. Li L, Karanika S, Yang G *et al.* Androgen receptor inhibitor-induced BRCAness and PARP inhibition are synthetically

lethal for castration-resistant prostate cancer. *Sci Signal* 2017;**10**:eaam7479. https://doi.org/10.1126/scisignal.aam7479
16. Asim M, Tarish F, Zecchini HI *et al.* Synthetic lethality between androgen receptor signalling and the PARP pathway in prostate cancer. *Nat Commun* 2017;**8**:374. https://doi.org/10.1038/s41467-017-00393-y
17. Siddiqui ZA, Krauss DJ. Adjuvant androgen deprivation therapy for prostate cancer treated with radiation therapy. *Transl Androl Urol* 2018;**7**:378–89. https://doi.org/10.21037/tau.2018.01.06
18. Longoria O, Beije N, de Bono JS. PARP inhibitors for prostate cancer. *Semin Oncol* 2023;**51**:25–35.
19. Jamal K, Galbiati A, Armenia J *et al.* Drug–gene interaction screens coupled to tumor data analyses identify the most clinically relevant cancer vulnerabilities driving sensitivity to PARP inhibition. *Cancer Res Commun* 2022;**2**:1244–54. https://doi.org/10.1158/2767-9764.CRC-22-0119
20. Crafter C, Vincent JP, Tang E *et al.* Combining AZD8931, a novel EGFR/HER2/HER3 signalling inhibitor, with AZD5363 limits AKT inhibitor induced feedback and enhances antitumour efficacy in HER2-amplified breast cancer models. *Int J Oncol* 2015;**47**:446–54. https://doi.org/10.3892/ijo.2015.3062
21. Loewe S, Muischnek H. Über kombinationswirkungen. *Archiv F Experiment Pathol u Pharmakol* 1926;**114**:313–26. https://doi.org/10.1007/BF01952257
22. Dobin A, Davis CA, Schlesinger F *et al.* STAR: ultrafast universal RNA-seq aligner. *Bioinformatics* 2013;**29**:15–21. https://doi.org/10.1093/bioinformatics/bts635
23. Liao Y, Smyth GK, Shi W. featureCounts: an efficient general purpose program for assigning sequence reads to genomic features. *Bioinformatics* 2014;**30**:923–30. https://doi.org/10.1093/bioinformatics/btt656
24. Love MI, Huber W, Anders S. Moderated estimation of fold change and dispersion for RNA-seq data with DESeq2. *Genome Biol* 2014;**15**:550. https://doi.org/10.1186/s13059-014-0550-8
25. Korotkevich G, Sukhov V, Budin N *et al.* Fast gene set enrichment analysis. bioRxiv, https://doi.org/10.1101/060012, 1 February 2021, preprint: not peer reviewed.
26. Subramanian A, Tamayo P, Mootha VK *et al.* Gene set enrichment analysis: a knowledge-based approach for interpreting genome-wide expression profiles. *Proc Natl Acad Sci USA* 2005;**102**:15545–50. https://doi.org/10.1073/pnas.0506580102
27. Carnevalli LS, Sinclair C, Taylor MA *et al.* PI3Kα/δ inhibition promotes anti-tumor immunity through direct enhancement of effector CD8(+) T-cell activity. *J Immunotherap Cancer* 2018;**6**:158. https://doi.org/10.1186/s40425-018-0457-0
28. Kordon MM, Zarębski M, Solarczyk K *et al.* STRIDE—A fluorescence method for direct, specific in situ detection of individual single- or double-strand DNA breaks in fixed cells. *Nucleic Acids Res* 2020;**48**:e14. https://doi.org/10.1093/nar/gkz1118
29. Illuzzi G, Staniszewska AD, Gill SJ *et al.* Preclinical characterization of AZD5305, A next-generation, highly selective PARP1 inhibitor and trapper. *Clin Cancer Res* 2022;**28**:4724–36. https://doi.org/10.1158/1078-0432.CCR-22-0301
30. Balmus G, Pilger D, Coates J *et al.* ATM orchestrates the DNA-damage response to counter toxic non-homologous end-joining at broken replication forks. *Nat Commun* 2019;**10**:87. https://doi.org/10.1038/s41467-018-07729-2
31. Adams DJ, Barlas B, McIntyre RE *et al.* Genetic determinants of micronucleus formation in vivo. *Nature* 2024;**627**:130–6. https://doi.org/10.1038/s41586-023-07009-0
32. Cruz C, Castroviejo-Bermejo M, Gutiérrez-Enríquez S *et al.* RAD51 foci as a functional biomarker of homologous recombination repair and PARP inhibitor resistance in germline BRCA-mutated breast cancer. *Ann Oncol* 2018;**29**:1203–10.
33. Ciccia A, Elledge SJ. The DNA damage response: making it safe to play with knives. *Mol Cell* 2010;**40**:179–204. https://doi.org/10.1016/j.molcel.2010.09.019
34. Kounatidou E, Nakjang S, McCracken SRC *et al.* A novel CRISPR-engineered prostate cancer cell line defines the AR-V transcriptome and identifies PARP inhibitor sensitivities. *Nucleic Acids Res* 2019;**47**:5634–47. https://doi.org/10.1093/nar/gkz286
35. Hasterok S, Scott TG, Roller DG *et al.* The androgen receptor does not directly regulate the transcription of DNA damage response genes. *Mol Cancer Res* 2023;**21**:1329–41. https://doi.org/10.1158/1541-7786.MCR-23-0358
36. Hussain M, Daignault-Newton S, Twardowski PW *et al.* Targeting androgen receptor and DNA repair in metastatic castration-resistant prostate cancer: results from NCI 9012. *JCO* 2018;**36**:991–9. https://doi.org/10.1200/JCO.2017.75.7310
37. Hussain MHA, Kocherginsky M, Agarwal N *et al.* BRCAAway: a randomized phase 2 trial of abiraterone, olaparib, or abiraterone + olaparib in patients with metastatic castration-resistant prostate cancer (mCRPC) bearing homologous recombination-repair mutations (HRRm). *JCO* 2024;**42**:19. https://doi.org/10.1200/JCO.2024.42.4_suppl.19
38. Chi KN, Rathkopf D, Smith MR *et al.* Niraparib and Abiraterone acetate for metastatic castration-resistant prostate cancer. *JCO* 2023;**41**:3339–51. https://doi.org/10.1200/JCO.22.01649

Received: January 23, 2025. **Revised:** July 30, 2025. **Accepted:** August 20, 2025
© The Author(s) 2025. Published by Oxford University Press.
This is an Open Access article distributed under the terms of the Creative Commons Attribution-NonCommercial License (https://creativecommons.org/licenses/by-nc/4.0/), which permits non-commercial re-use, distribution, and reproduction in any medium, provided the original work is properly cited. For commercial re-use, please contact reprints@oup.com for reprints and translation rights for reprints. All other permissions can be obtained through our RightsLink service via the Permissions link on the article page on our site—for further information please contact journals.permissions@oup.com.